Progress In Electromagnetics Research Letters, Vol. 50, 7–12, 2014

3D Millimeter Wave Image by Combined Active and Passive System

Xuan Lu[1], Zelong Xiao[1, *], Jianzhong Xu[1], and Haiqiang Huo[2]

Abstract—This paper presents a data fusion algorithm combining a 24 GHz radar and a 94.5 GHz radiometer for 3D image. Three trihedral reflectors are tested as multiple targets. Based on a conical scanner, the radar azimuth-range image and radiometric azimuth-elevation image are firstly obtained and preprocessed respectively. Then the common dimension of azimuth is made use of to align two images and synthesize a 3D image, where the positions, ranges and combined intensities of the targets are illustrated. Outdoor tests and experiment results demonstrate the effectiveness of the idea.

1. INTRODUCTION

Millimeter wave (MMW) system is demonstrated to have better performance than infrared or visible systems in poor weather or battlefield conditions, thus both active and passive MMW techniques are very important for civil and military applications [1–3]. The active radar offers distant operation, high range resolution, and precise speed information by transmitting a well designed electromagnetic wave. However, it suffers from speckle and glint in short range and is easy to be interfered by enemy. On the other hand, the passive system, radiometer, is an ultra wide band receiver with high sensitivity. It receives the thermal signal depending on the emissivity and reflectivity of the object rather than transmitting wave. It is harmless to human being, free of speckle and glint, and it remains covert to enemy but is powerless in range and speed sensing.

In this paper, we combine a 24 GHz LFMCW (linear frequency modulated continuous wave) radar and a 94.5 GHz total power radiometer, and research active and passive image fusion. The motivation is that the range information for the radar and the radiometric characteristic for the radiometer provide a potential probability of generating 3D image by taking advantage of the two sensors. The difficulty in this case is that the sensors are not of compatible dimensionality because the radar image differs in three major ways from the general concept of image. Firstly, radar detects range information which the radiometer cannot provide. Secondly, passive sensor provides only the intensity of the first object along the ray corresponding to any particular pixel. Last but not least, the resolutions of the two sensors are quite different [4].

2. SYSTEM CONSTRUCTION AND BASIC PRINCIPLES

A schematic diagram of the combined radar and radiometer system mounted on a conical scanner and photos of principal components can be seen in Fig. 1. The scanner is directed by the scan controller which transfers user instructions through RS-232 port. The radiometer is equipped with a Cassegrain antenna while the radar is with a planner array antenna. The raw data of the radiometer and radar are collected by a commercial ADC circuit and transferred to an industrial personal computer (IPC) through PCI interface. The performance characteristics of the system [5, 6] are summarized in Table 1.

Received 4 September 2014, Accepted 29 October 2014, Scheduled 8 November 2014

* Corresponding author: Zelong Xiao (zelongxiao@mail.njust.edu.com).

[1] School of Electronic and Optical Engineering Nanjing University of Science and Technology, Nanjing, China. [2] The 54th Research Institute of China Electronics Technology Group Corporation, Shijiazhuang, China.

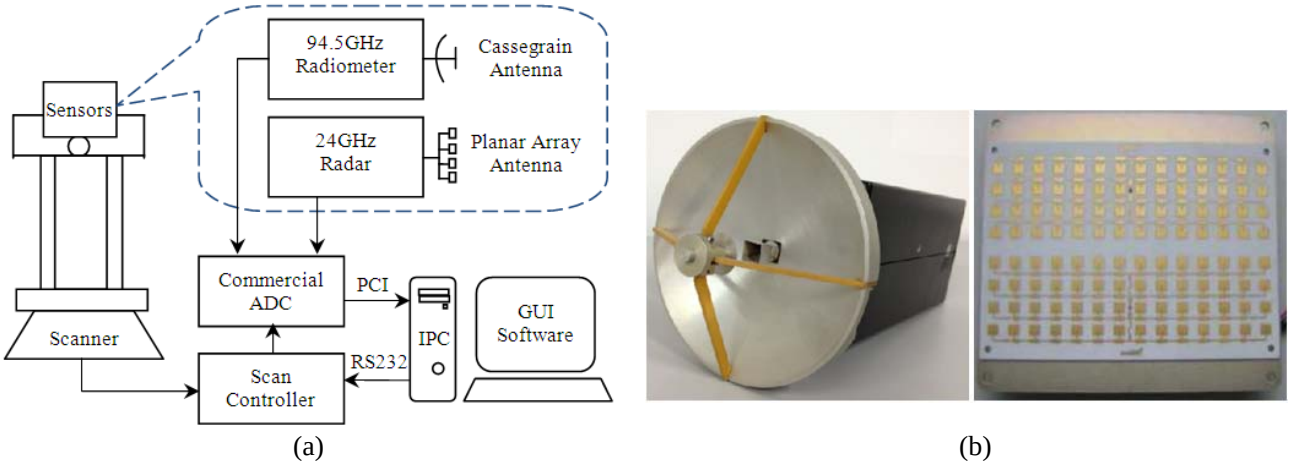

Figure 1. (a) Schematic diagram of the combined system and photos of (b) the 94.5 total power radiometer, and (c) the 24 GHz LFMCW radar antenna.

Table 1. Radar and radiometer performance characteristics.

	Parameter	Value
radar (Standard Value)	FM mode	Triangular
	Center frequency	24 GHz
	FM bandwidth	250 MHz
	Output power	20 dBm
	FM frequency	100 Hz∼2 kHz
	IF bandwidth	50 Hz∼150 kHz
	Antenna size	105 mm × 85 mm
	Beam width	7° azimuth × 28° elevation
radiometer (Measured Value)	Mode	Total power direct detection
	Center frequency	94.5 GHz
	IF bandwidth	500 MHz∼2 GHz
	Sensitivity	0.4 K
	Antenna aperture	145 mm
	3dB Beam width	Symmetrically 1.5°
Scanner	Azimuth range	−170°∼170°
	Elevation range	−75°∼75°
ADC	Max sample frequency	330 kHz

2.1. High Range Resolution Profile for LFMCW Radar

The LFMCW radar design uses triangular or saw tooth modulation to get high range resolution which is basically smaller than the interested target. The frequency varies with a constant rate of change during either the up- or down-ramps of the triangle wave. The echo generated by target scattering is delayed by the round trip time. Then the frequency difference between the transmitted and received signal is a constant for a target at a fixed range. For a target at a greater distance, the echo is delayed more, and the difference frequency, f_b, is higher. Therefore, the difference frequency is proportional to

the range, R, of a stationary target [7]. Specifically, it is calculated as

$$f_b = \frac{4\Delta F}{T_p c} \cdot R \tag{1}$$

where ΔF denotes the FM bandwidth, T_p the duration of one up-ramp and one down-ramp, and c the constant of light velocity. As a result, the target and its range can be extracted from the frequency spectrum of the difference signal, while the range resolution, δR, depends on the FM bandwidth by $\frac{c}{2\Delta F}$.

In this paper, the radar is equipped by a fan beam antenna, which does not perform spatial resolution at elevation dimension. Thus the radar is scanned once in azimuth dimension to generate a 2D image with axes of azimuth-range.

2.2. Effective Radiometric Temperature for the Radiometer

Passive MMW detection is categorized to thermal techniques similar to infrared mechanism. A radiometer receives radiation both reflected and emitted by the objects in the line of sight. For a non-transparent object, the emissivity and reflectivity are related through $\varepsilon + r = 1$. The effective radiometric temperature contributed by object emission, also known as the object's surface brightness, equals its thermodynamic temperature, T_0, multiplied by its emissivity. And the contribution reflected from the object is defined as the product of the object reflectivity and the radiometric illumination temperature, T_{ill}. Combining the two parts, the effective radiometric temperature T_e of the object can be expressed as [8]

$$T_e = \varepsilon \cdot T_0 + r \cdot T_{ill} \tag{2}$$

For a pencil beam single pixel sensor, the radiometer is progressively scanned in azimuth and elevation dimensions to generate a 2D intensity image. The radiometric temperature difference between pixels holds the clue to the information of the target.

2.3. 3D Image by Active and Passive Data Fusion

3D image is achieved by fusing the radar range profiles and radiometric temperatures of a scene:

- Firstly obtain the raw data of two sensors. For the radar, it only works during the first scan in azimuth dimension due to the fan beam. The radar return signal is recorded at every azimuth angle and processed by FFT operation to get the range profile at this azimuth. Then the range profile is arranged to generate a 2D azimuth-range image. Regarding to the radiometer, the radiometric temperature of the scene is recorded at every sampled direction controlled by the conical scanner to generate an radiometric azimuth-elevation image.
- Normalize and threshold segment for two images. This process is to extract the target region and eliminate the influence of background noise and side lobe for radar range profiles. The values of the target regions are saved while others are assigned to be zeros. Proper denoising and image enhancing technique for radiometric image can be preprocessed before this stage.
- Span 3D image by fusing two images. As the sensors are not of compatible dimensionality, we make use of the azimuth information which is aligned and shared by the two images and span a 3D space of azimuth-elevation-range. Specifically, (1) for an nonzero pixel in the radiometric image, label its azimuth angle and record the radiometric temperature; (2) check the radar range profile at this azimuth angle and search all the nonzero values, record their ranges and profile intensities; (3) in the 3D range-azimuth-elevation coordinate system, the fused value is only assigned for points selected in step (2) by the root mean square of radar profile intensity and radiometric temperature, while the fused values are zeros for other points.
- Finally, transfer the 3D image to Cartesian coordinate system according to the relation with spherical coordinates.

3. EXPERIMENT

Outdoor experiments are carried out with three trihedral reflectors to be tested targets as shown in Fig. 2(a). The 24 GHz real aperture radar and the single pixel 94.5 GHz radiometer are mounted on the conical scanner at heights of 1.95 m and 1.8 m, respectively, while the heights of the reflectors are all set by 0.8 m. The relative locations of the scanner and the reflectors are shown in Fig. 2(b). Then the ranges between the radar and Trihedral A, B and C are respectively 2.80 m, 2.31 m and 1.96 m. The measured FM bandwidth is 225 MHz, and FM frequency is set to be 0.5 kHz. The range resolution of the radar is calculated 0.67 m. In this paper, the three targets are not in the same radar line of sight, and the three targets is distinguishable although their range differences are smaller than 0.67 m. According to Equation (1), the corresponding difference frequencies of the targets are ranged from about 2.9 kHz to 4.5 kHz. The sample frequency is set as 50 kHz to acquire reasonable data volume but accumulate adequate energy for every 1024 points for FFT operation.

The view of interest is progressively scanned every 0.1° in azimuth by elevation interval of 1°. As discussed in Section 2, radar signal is recorded once in an azimuth trip with 1024 points for every azimuth angle due to the fan beam, while the intensities of the radiometric temperature are recorded during all the scanning procedure. The radar range profile is calculated azimuth-by-azimuth, and arranged to generate a 2D azimuth-range image. As for the radiometric image, it is ten times linearly interpolated in elevation dimension before morphological filtering for a trade-off between imaging time and pixel resolution. Then the object areas of both images are extracted by a threshold. The raw data and

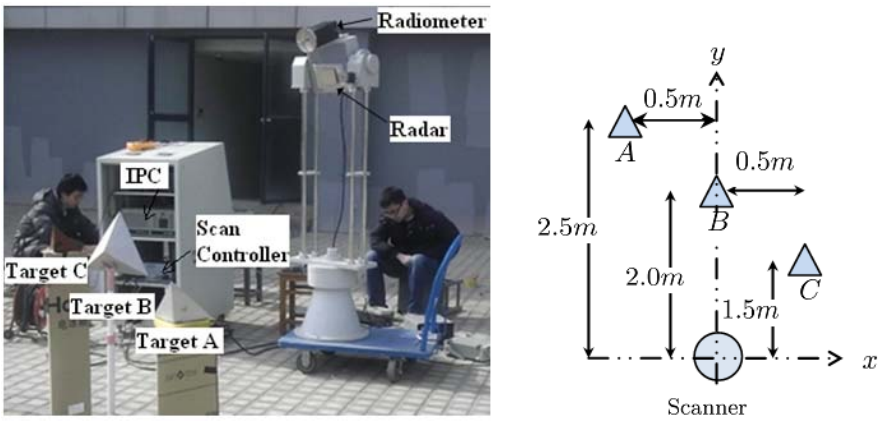

Figure 2. (a) Outdoor experiment set up and (b) relative locations of the scanner and the reflectors.

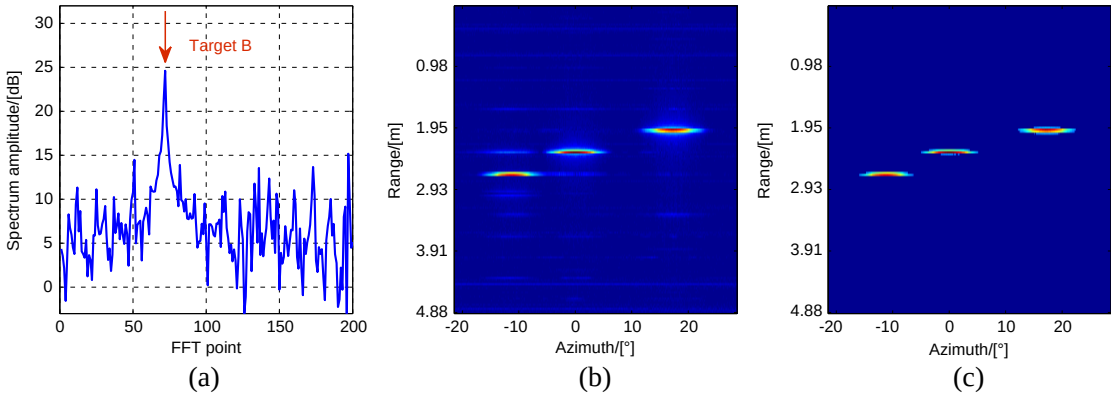

Figure 3. Measured and processed radar data: (a) radar range profile at azimuth angle of zero degree, (b) the arranged 2D azimuth-range image, and (c) object regions extracted by a threshold.

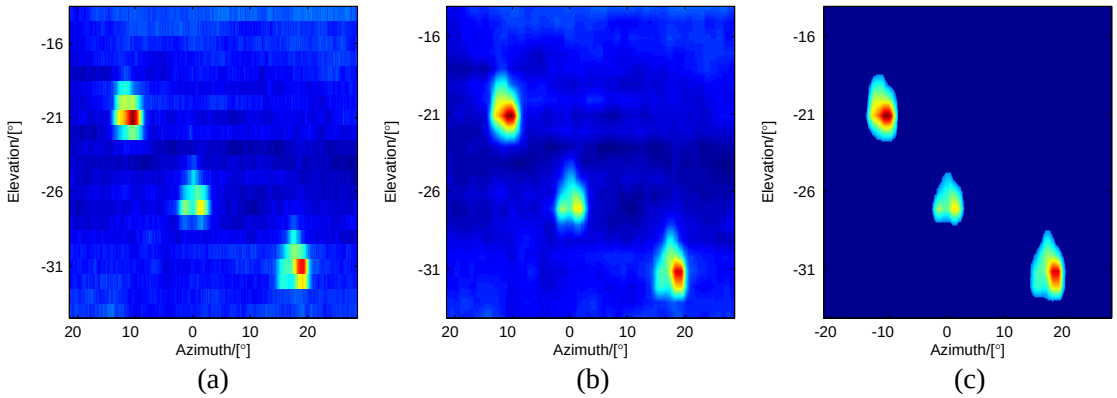

Figure 4. Measured and processed radiometer data: (a) raw data, (b) radiometric image after interpolation and filtering processing, and (c) object regions extracted by a threshold.

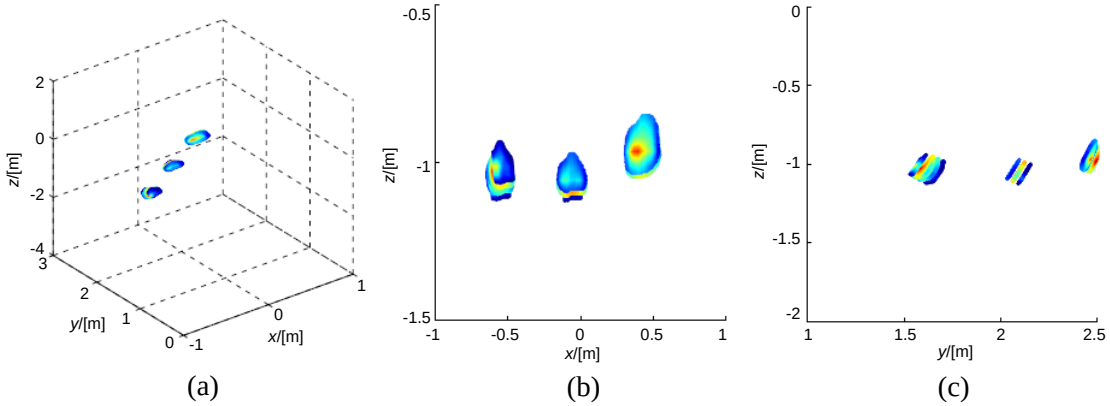

Figure 5. Combined radar and radiometer data result: (a) 3D image, (b) front view, and (c) left view.

processed images for radar and radiometer can be seen in Fig. 3 and Fig. 4, respectively.

Fig. 3(a) shows the radar range profile at azimuth of zero degree. In this case, only target B is illuminated in radar beam, and the main lobe is 10 dB higher than the first side lobe. The profiles at all azimuths are calculated and arranged to compose the azimuth-range image, as shown in Fig. 3(b), where all of the three targets are located in azimuth and range dimensions. Image in Fig. 3(c) ignores the side lobes and noises by a threshold and obtains the final azimuth-range image for fusion with passive data. Fig. 4(a) shows the raw data of the radiometer recorded in two dimensions of azimuth and elevation, which is sequentially processed by linear interpolation, morphological filtering, and threshold processing (see Fig. 4(b) and Fig. 4(c)) before data fusion with radar image.

The 3D result of combined radar and radiometer image is shown in Fig. 5(a) in an x-y-z Cartesian coordinate system, while its front view and lateral view are shown in Fig. 5(b) and Fig. 5(c), respectively. The local maximum values of the target regions are coordinated by $(-0.57, 1.59, -1.02)$, $(-0.08, 2.08, -1.07)$, and $(0.42, 2.49, -0.98)$, demonstrating the effectiveness of our method.

4. CONCLUSION

Data fusion of combined MMW radar and radiometer system for 3D image is realized in this paper. Based on a conical scanner in azimuth and elevation dimension, radar azimuth-range image and radiometric azimuth-elevation image for multiple targets of three trihedral reflectors are obtained. Making use of azimuth angle that is common to both images, the proposed algorithm is demonstrated capable to synthesize a 3D image, where the position, range and combined intensity of the targets are well illustrated.

ACKNOWLEDGMENT

This paper was supported by National Nature Science Foundation of China (No. 61301213), the Natural Science Foundation of Jiangsu Province, China (Fund No. BK20130768) and the Fundamental Research Funds for Ministerial Key Laboratory of JMT, Nanjing University of Science and Technology (No. 3092013012200Y).

REFERENCES

1. Yujiri, L., "Passive millimeter wave imaging," *Proc. IEEE MTT-S International Microwave Symposium Digest*, 98–101, 2006.
2. Brooker, G., R. Hennessey, M. Bishop, C. Lobsey, and A. Maclean, "Millimetre wave 3D imaging for industrial applications," *Proc. Wireless Broadband and Ultra Wideband Communications and 2nd International Conference on AusWireless*, 27–30, 2007.
3. Mizuno, K., H. Matono, Y. Wagatsuma, H. Warashina, H. Sato, S. Miyanaga, and Y. Yamanaka, "New applications of millimeter-wave incoherent imaging," *Proc. IEEE MTT-S International Microwave Symposium Digest*, 12–17, 2005.
4. Grover, R., G. Brooker, and H. F. Durrant-Whyte, "Environmental representation for fused millimetre wave radar and nightvision data," *Proc. International Conference on Control, Automation, Robotics and Vision (ICARCV 02)*, 7–12, 2002.
5. Hu, T., "Methods of indoor millimeter-wave radiometric imaging for personnel concealed contraband detection," Ph.D. Thesis, Nanjing University of Science and Technology, Jun. 2012.
6. Data Sheet, Available at: http://www.innosent.de/en/industry/green-line-radarsensor/ivs-179/.
7. Wadge, G., D. G. Macfarlane, D. A. Robertsonb, A. J. Hale, H. Pinkertonc, R. V. Burrell, G. E. Nortond, and M. R. James, "AVTIS: A novel millimetre-wave ground based instrument for volcano remote sensing," *Journal of Volcanology and Geothermal Research*, Vol. 146, 307–318, 2005.
8. Kim, W. G., N. W. Moon, H. K. Kim, and Y. H. Kim, "Linear polarization sum imaging in passive millimeter-wave imaging system for target recognition," *Progress In Electromagnetics Research*, Vol. 136, 175–193, 2013.